Journal of
Materials Chemistry B

PAPER

View Article Online
View Journal | View Issue

Cite this: J. Mater. Chem. B, 2016, 4, 2466

Multicolour fluorescent carbon nanoparticle probes for live cell imaging and dual palladium and mercury sensors†

Vinay Sharma,[a] Anoop Kumar Saini[b] and Shaikh M. Mobin*[abc]

Received 27th January 2016,
Accepted 8th March 2016

DOI: 10.1039/c6tb00238b

www.rsc.org/MaterialsB

Carbon based nanomaterials are emerging as a desirable alternative to semiconducting quantum dots due to their unique optical properties and biocompatibility. The present study demonstrates the design and synthesis of highly fluorescent carbon nanoparticles (CNPs). The CNPs are investigated for their biocompatibility and henceforth successfully employed as promising multicolor bioimaging probes in A375 and DU145 cell lines. Furthermore, a "turn off" mode has been established for the detection of noble metal palladium (Pd^{2+}) and heavy metal mercury (Hg^{2+}) by quenching the fluorescence of CNPs. The CNP sensor responded to the detection of Pd^{2+} (5–100 μM) and Hg^{2+} (1–18 μM) in a wide range with the limit of detection (LOD) of 58 nM for Pd^{2+} and 100 nM for Hg^{2+}. The CNP sensor was employed for the detection of Pd^{2+} and Hg^{2+} in real water samples and detection of leftover palladium catalysts in a model reaction system. Also, the CNPs were successfully employed as intracellular mercury and palladium sensors using confocal microscopy.

Introduction

Carbon nanomaterials have shown promising fluorescence properties with carbon dots (CDs) leading the race for sensing applications of biomolecules such as enzymes or nucleic acids to trace metal ion detection due to their unique optical properties.[1] Carbon based nanoparticles are found to have advantages over traditional semiconducting quantum dots due to their reduced toxicity.[2] Cytotoxicity associated with fluorescent semiconducting quantum dots is the bottleneck for real life applications, thus exploring new strategies for large scale synthesis of carbon nanoparticles (CNPs) in high quantum yield with low toxicity is still a challenge. Along with the highly fluorescent nature, hydrophilicity is one of the most important characteristics of these CNPs which makes them suitable for bioimaging applications. These CNPs can be treated as a potential replacement for cadmium and selenium based nanomaterials used in *in vitro* and *in vivo* cellular imaging.[3] Multicolour fluorescence emission is also one of the most important properties of these CNPs and much effort has recently been made to synthesize carbon based nanomaterials for bioimaging.[4–7]

Palladium is a rare transition noble metal which belongs to the Pt group and plays an important role in various biological and chemical activities. Palladium (Pd) has applications in dental crowns, cancer treatment, jewellery, medical instruments, electronics and many others.[8] Pd^{2+} is also used as a catalyst in various chemical reactions and the contamination of Pd^{2+} left in reaction products requires extensive purification.[9] The residue of Pd^{2+} left in water, food or drugs can cause adverse effects on health, hence the detection of Pd^{2+} is of considerable interest. The conventional methods for Pd detection, such as X-ray fluorescence, atomic absorption spectroscopy (AAS), plasma emission spectroscopy and high performance liquid chromatography (HPLC),[10] suffer from high instrument cost and rigorous experimental conditions. Thus, a simple, easy and rapid methodology for the determination of Pd^{2+} in solutions has been accorded significant attention. Although few fluorogenic probes have been synthesized recently for palladium detection studies based on their cytotoxicity and intracellular applicability are rare.[11]

Heavy metal mercury is known for its toxic impacts in all its oxidation states,[12] hence a real time detection system for mercury is of practical importance. Currently, fluorescence based sensors are very popular because of their simplicity, non-destructive nature and rapid analysis.[13] A few fluorescence turn off sensors have been already reported for Hg detection using carbon based nanomaterials,[14–16] even though many are efficient and selective the studies are targeted almost exclusively on Hg^{2+} ions. However, so far no reports have been available on Pd^{2+} and Hg^{2+} dual sensors.

[a] Centre for Biosciences and Bio-Medical Engineering, Indian Institute of Technology Indore, Simrol, Indore-452020, India. E-mail: xray@iiti.ac.in
[b] Discipline of Chemistry, Indian Institute of Technology Indore, Simrol, Indore-452020, India
[c] Centre for Material Science and Engineering, Indian Institute of Technology Indore, Simrol, Indore-452020, India

† Electronic supplementary information (ESI) available. See DOI: 10.1039/c6tb00238b

Herein, we report a simple, low cost synthesis strategy for carbon nanoparticles (CNPs) having advantages such as large scale production, high quantum yield and low cytotoxicity. Furthermore, the CNPs exhibited a sensitive, selective and rapid sensing response to the detection of Pd^{2+} and Hg^{2+} in real life samples along with the potential of a multicolor bio-imaging probe and intracellular sensing.

Results and discussion

Highly fluorescent carbon nanoparticles (CNPs) were synthesized by a hydrothermal method employing citric acid as a carbon source in aqueous media. The potential of CNPs as efficient sensors for noble metal Pd^{2+} and heavy metal Hg^{2+} (Scheme 1) was explored. Also, its applicability as a multicolor cell-labelling probe was studied.

Characterization of carbon nanoparticles (CNPs)

The structural and optical properties of CNPs were investigated using powder X-ray diffraction (PXRD), Fourier-transform infrared spectroscopy (FT-IR), scanning electron microscopy (SEM), UV-visible, fluorescence spectroscopy and time correlated single photon counting (TCSPC).

The XRD pattern of CNPs shown in Fig. 1(a) exhibited a broad diffraction peak at $2\theta = 23.8^{\circ}$ representing poor crystallinity. The corresponding *d*-spacing was found to be 3.7 Å, which was larger than the lattice spacing between graphite 002 planes.[17] The UV-visible absorption spectrum of CNPs shows a typical absorption peak corresponding to n–π* transition of C═C at 233 nm and a peak corresponding to π–π* transition of C═O at 340 nm[18] (Fig. 1(b)). The optimum excitation and emission wavelengths of the as-synthesized CNPs were found to be 340 and 440 nm, respectively. The SEM image of CNPs presented in Fig. 1(c) exhibits the nearly spherical morphology of carbon nanoparticles with a particle size of 8–12 nm, which includes some aggregation.

Fourier transform infrared spectroscopy (FT-IR) was performed to identify the functional groups on the CNP. The FT-IR spectra of CNPs in Fig. 1(d) exhibit peaks at 1650 cm^{-1}, 1554 cm^{-1}, 1210 cm^{-1} and 1020 cm^{-1}, which are attributed to C═O, N–H, C–C and C—O, respectively.[19,20] The peak observed at 1380 cm^{-1} could be indicative of a C–O–C asymmetric stretch.[21] The broad peak at 3440 cm^{-1} provides evidence for the existence of N–H and –OH which results in the enhanced stability and hydrophobic nature of CNPs in aqueous media.[22] The photoluminescence spectra of CNPs exhibited in Fig. 1(e) represent the maximum emission at 440 nm. The fluorescence lifetime decay profile of CNPs shows triple exponential kinetics and is presented in Fig. 1(f). The average lifetime (τ) was calculated to be 7.95 ns which is in accordance with earlier reports.[2] Such a short lifetime is also an indicative of the radiative recombination of excitons leading to fluorescence[23] (Table S1, ESI†).

The quantum yield of the as-synthesized CNPs at an excitation wavelength of 340 nm was calculated to be 24.9% using quinine sulphate (QY = 54%) as a standard. It is worth mentioning that although the obtained quantum yield is less compared to the CDs synthesized by laser ablation it is significantly higher than that of the CDs synthesized either by carbonisation of polymers[24] and carbohydrates[25,26] or by electrochemical methods.[27]

Fluorescence stability of CNPs

To evaluate the stability of the as-synthesized CNPs under harsh conditions, various experiments were performed. The relative activity of fluorescence at different pH values is shown in Fig. 2(a). It can be seen that the CNPs are stable in a wide range of pH values (4–12). However, under highly acidic conditions (below pH 3) approximately 50% decrease in relative fluorescence intensity at pH 2 was observed (Fig. 2(a)). A clear shift in absorption and emission spectra was seen at pH 2 and pH 3 (Fig. S1, ESI†). The stability of CNPs was tested in different temperature ranges and the fluorescence intensity was found to be almost stable in the temperature range of −20 to 90 °C as depicted in Fig. 2(b).

Furthermore, fluorescence stability of CNPs was tested using two different methods: (i) by illuminating CNPs with UV light using an UV lamp of 366 nm for two hours the change in

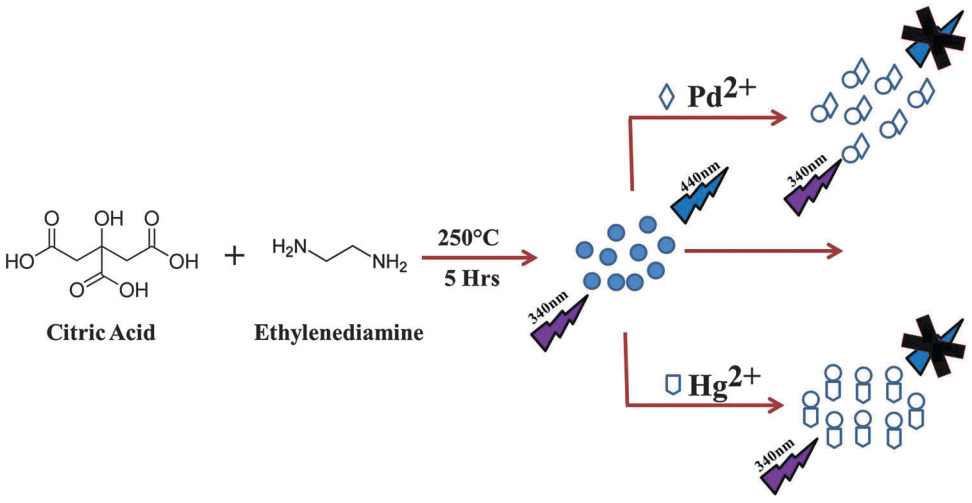

Scheme 1

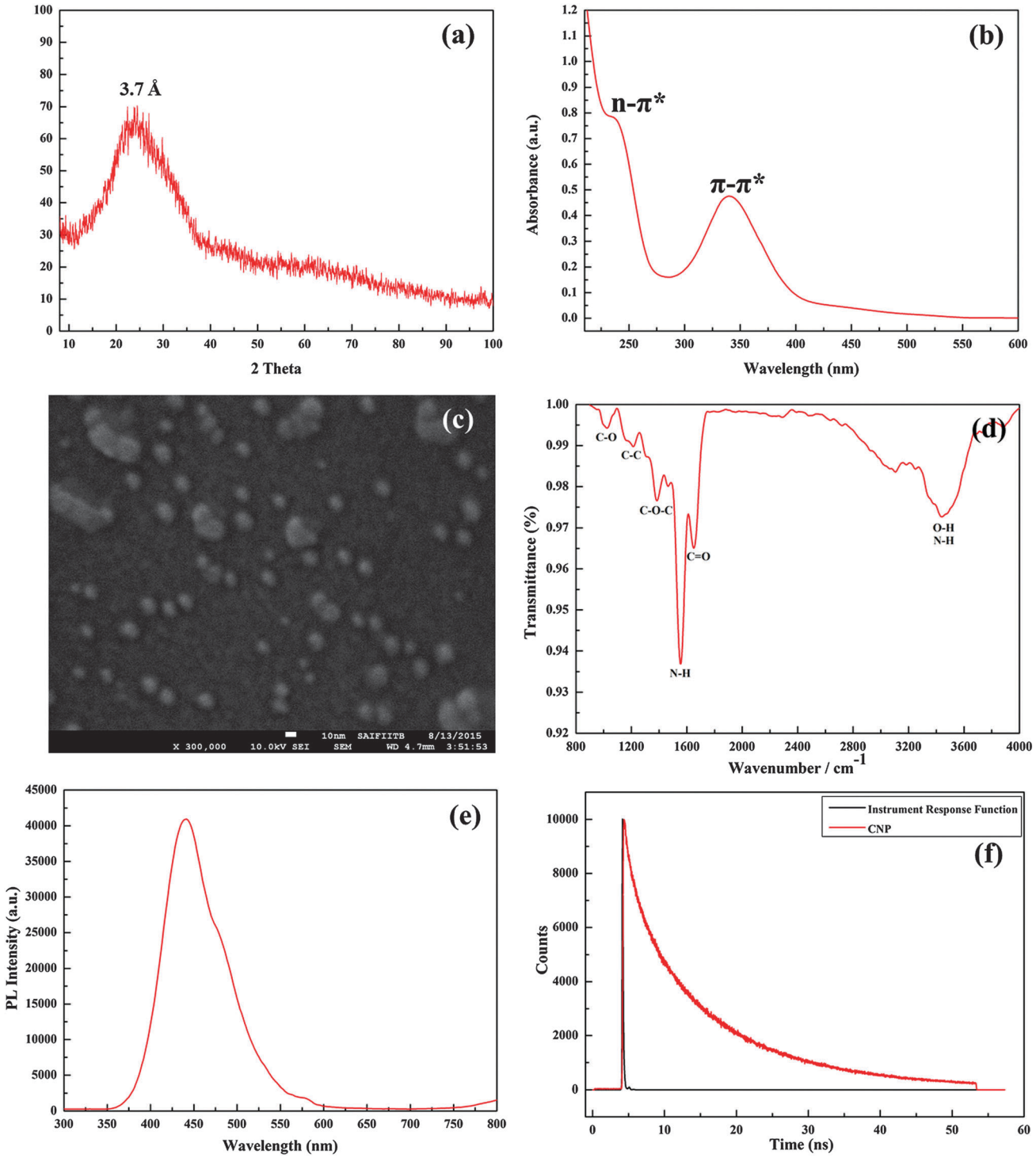

Fig. 1 Characterization of carbon nanoparticles: (a) powder X-ray diffraction, (b) UV-visible spectrum, (c) SEM image of CNPs, (d) FT-IR spectrum, (e) photoluminescence spectrum, and (f) lifetime decay curve.

fluorescence intensity was recorded every 10 minute interval. This results in a continuous decay in intensity up to 75.2% in 2 hours (Fig. 2(c)) indicating the instability of CNP fluorescence under continuous UV illumination. (ii) By keeping CNPs at room temperature, no changes were observed for a period of approximately 30 days, which represents good stability (Fig. 2(d)). This makes CNPs best candidates for room temperature sensing applications.

Fluorescence sensing of Pd^{2+} and Hg^{2+}

The sensing of noble metals is of considerable interest due to toxicity and expensiveness associated with these metal ions.

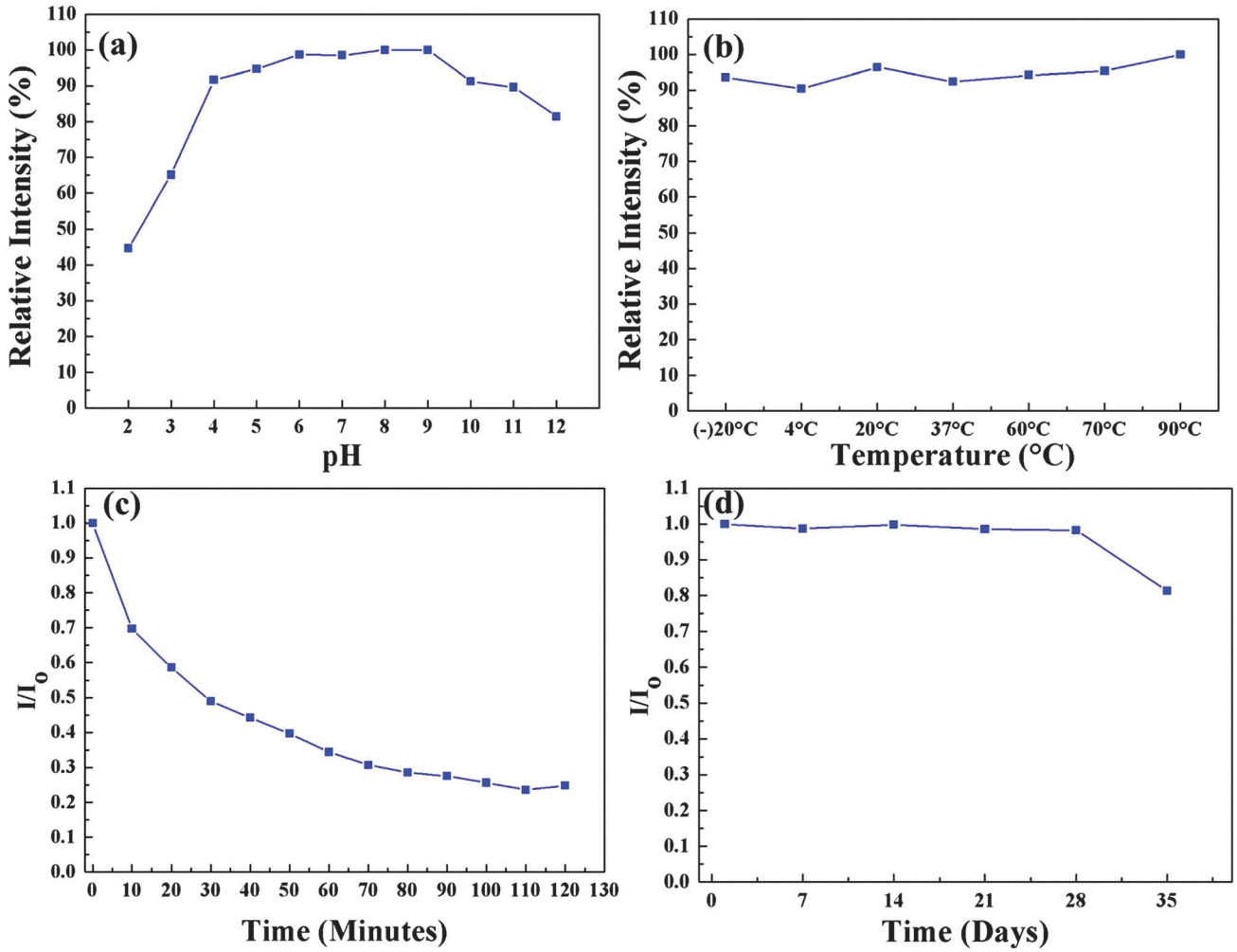

Fig. 2 Stability of fluorescence intensity at (a) varied pH, (b) varied temperature, (c) varied UV illumination, and (d) varied time.

The results of fluorescence titration of CNPs with increasing concentrations of Pd^{2+} and Hg^{2+} are shown in Fig. 3. The increasing concentration of Pd^{2+} from 0 to 100 μM in steps of 5 μM each leads to a consistent decay in fluorescence intensity and a total of 88.4% decay of the initial fluorescence intensity was found at 100 μM Pd^{2+} concentration. A linear response in the case of Pd^{2+} is detected in the range of 35–100 μM with the limit of detection as low as 58 nM. A similar kind of fluorescence decay was found when increasing the concentration of Hg^{2+} from 0 to 18 μM in steps of 1 μM each. A linear response was also exhibited in this range with the LOD as low as 100 nM. The total decay in fluorescence in the case of Hg^{2+} was 31.63% of the initial intensity. The fluorescence titration with lower concentrations of Pd^{2+} (500 nM–5 μM) and Hg^{2+} (400 nM–1 μM) is shown in Fig. S2 (ESI†).

The LOD is calculated using the following equation:[28]

$$\mathrm{LOD} = 3.3(\sigma/S) \quad (1)$$

where σ and S are the standard error and the slope of the calibration curve respectively.

The absorbance spectrophotometric titration was performed in water and it revealed that the gradual increase in the concentration of Pd^{2+} results in a decrease in absorption intensity of CNPs at 340 nm. When the concentration of CNPs was kept constant and Pd^{2+} was added in steps of 5 μM, two isosbestic points are obtained at 378 nm and 253 nm. A similar behaviour was observed in the case of increasing the amount of Hg^{2+} with two isosbestic points at 370 nm and 252 nm (Fig. 4). The absorbance titration further validates the sensing behaviour of CNPs.

It can be seen from Fig. 3 that although the detection emission wavelengths for Pd^{2+} and Hg^{2+} are the same they have a different non-interfering linear range of detection. Still, the individual identification of Pd^{2+} and Hg^{2+} is a challenge using only the fluorescence. However, the CNPs can selectively differentiate Pd^{2+} and Hg^{2+} from other metal ions using fluorescence turn off behaviour.

In order to understand the decay kinetics of CNPs in the presence of Pd^{2+} and Hg^{2+}, TCSPC experiments were conducted. As exhibited in Fig. 5 the average life time of CNPs which was found to be 7.95 ns was reduced to 2.53 ns with the addition of

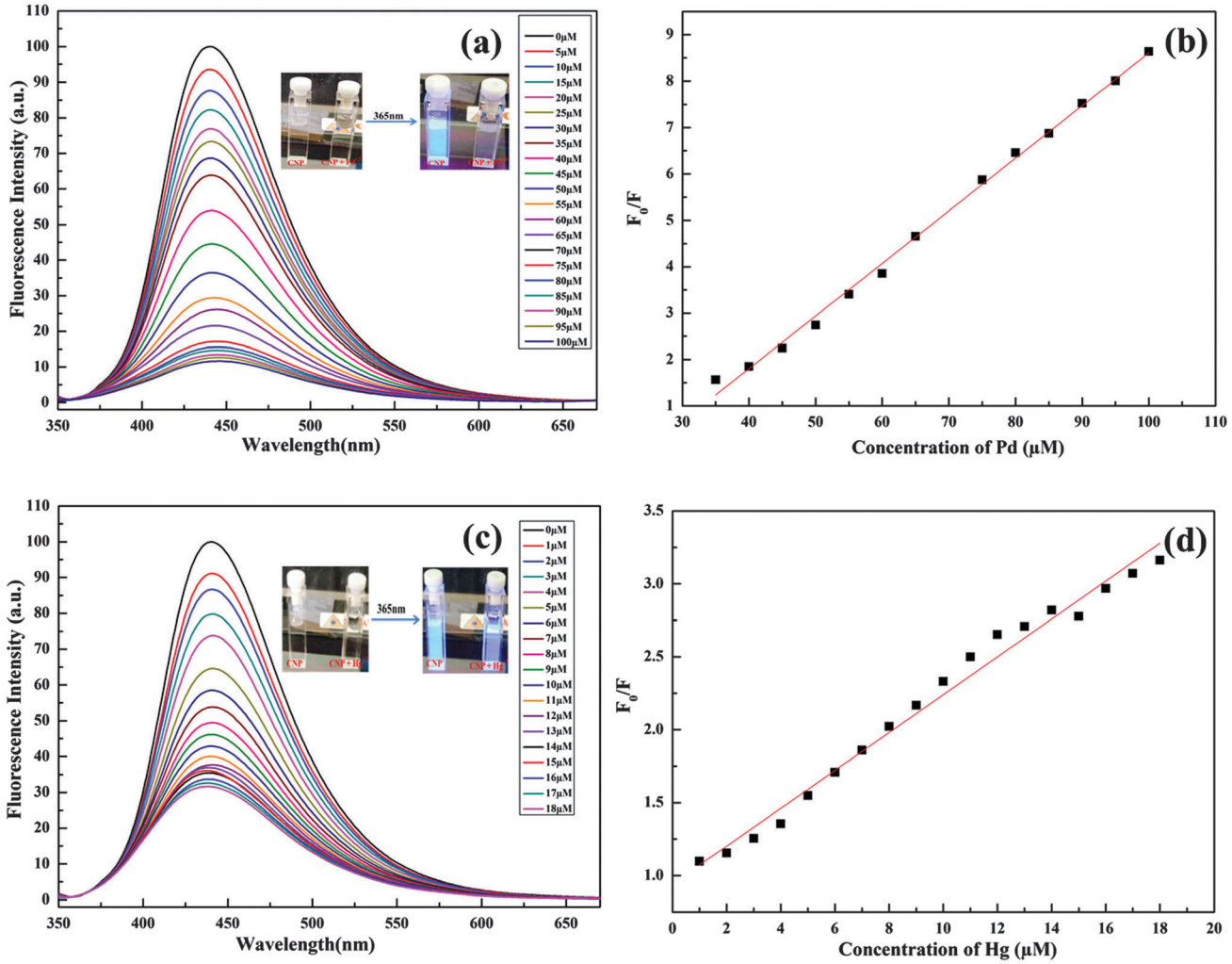

Fig. 3 Fluorescence quenching of CNPs in the presence of noble metals Pd and Hg. (a and b) In the presence of Pd^{2+} (0–100 μM). (c and d) In the presence of Hg^{2+} (0–18 μM).

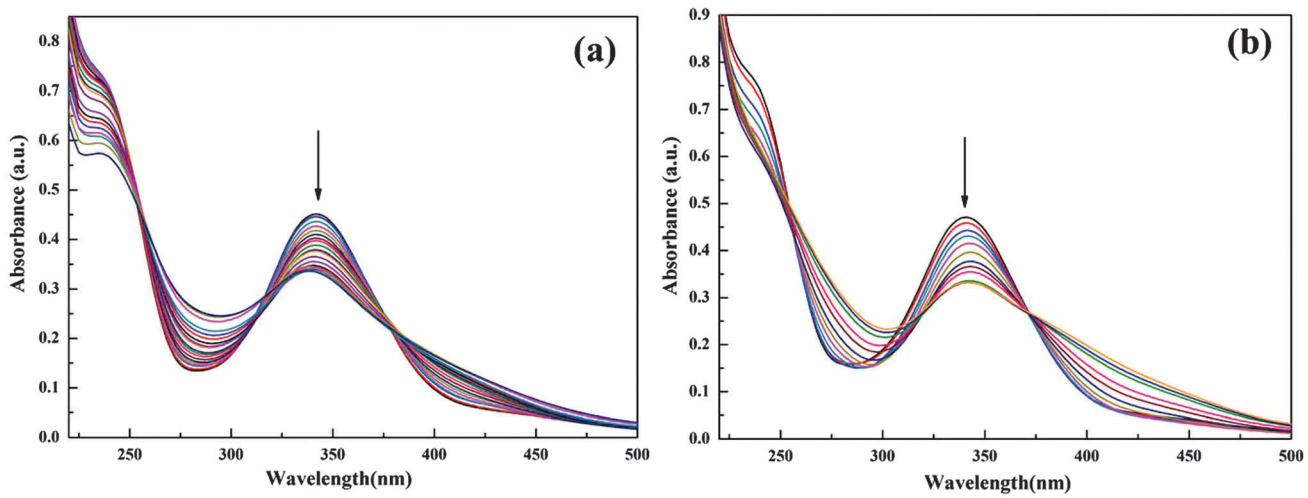

Fig. 4 Absorption titration of CNPs in the presence of noble metals Pd and Hg. (a) In the presence of Pd^{2+} and (b) in the presence of Hg^{2+}.

Hg^{2+}. The obvious reduction in fluorescence lifetime can be indicative of a very fast electron transfer process between CNPs and Hg^{2+} that led to dynamic quenching. On the other hand, the addition of Pd^{2+} does not result in any significant change in

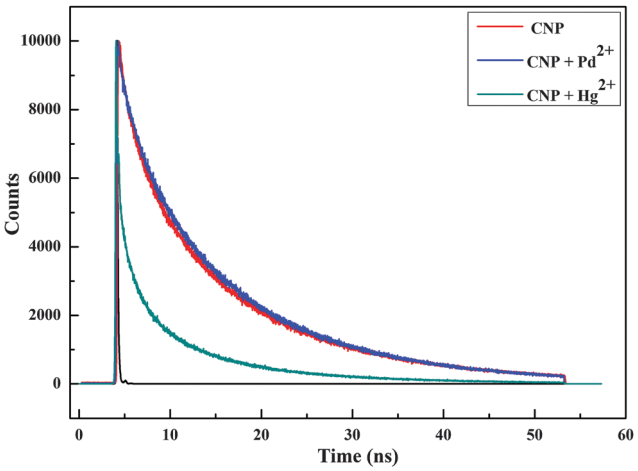

Fig. 5 Lifetime decay profile of CNPs in the presence of Pd^{2+} and Hg^{2+}.

fluorescence lifetime and it was found to be 7.94 ns. The almost similar average lifetimes indicate that non-radiative electron transfer does not occur and it is an indication of static quenching (Table S1, ESI†). The TCSPC could successfully differentiate between Pd^{2+} and Hg^{2+}; hence the challenge with individual identification of Pd^{2+} and Hg^{2+} could be successfully overcome using TCSPC (Chart S1, ESI†).

Specificity of the sensor

Besides sensitivity, specificity is another parameter to evaluate the performance of a sensor. In this regard, the selectivity of the sensor toward Pd^{2+} and Hg^{2+} was tested using other 19 representative metal ions under the same conditions as Pd^{2+} and Hg^{2+} and relative changes in fluorescence were recorded. It is noticeable from Fig. 6(a) that only Pd^{2+} and Hg^{2+} could have a considerable effect on the fluorescence intensity of the CNPs while other metal ions have much less or negligible effect. It is worth mentioning that the concentration used for other metal ions was thrice the concentration used for Pd^{2+} and Hg^{2+}. Furthermore, considering the applicability of CNPs as biosensors, their selectivity was tested in the presence of biomolecules including amino acids (l-cysteine, glycine and proline), proteins (bovine serum albumin (BSA) and human serum albumin (HSA)), nucleic acids (calf thymus DNA) and biothiol (glutathione). The selectivity profile is shown in Fig. 6(b) which exhibits a negligible effect of biomolecules on the selectivity of CNPs towards Pd^{2+} and Hg^{2+}.

In order to understand the practical ability of CNPs for the sensitive and selective detection of Pd^{2+} and Hg^{2+}, a competitive study was carried out in the presence of other metal ions. As illustrated in Fig. 7, the presence of other metal ions does not cause any considerable variation in the fluorescence behaviour of CNPs hence the CNPs act as selective chemosensors for Pd^{2+} and Hg^{2+} in the presence of other competitive metal ions.

Real sample analysis

To determine the feasibility of CNP sensors to probe Pd^{2+} and Hg^{2+} in real samples, their applicability was tested on tap water and reverse osmosis purified (R.O.) water. The method involves standard addition of Pd^{2+} and Hg^{2+} in real samples and determination of recovery based on fluorescence. The findings are summarised in Table 1, which represent that the CNP sensor is practical and sensitive for rapid detection of Pd^{2+} and Hg^{2+}.

Palladium is used as a catalyst in various reactions such as the Suzuki–Miyaura, Heck, Buchwald–Hartwig and Sonogashira reactions. We analyze the potential of the proposed sensor to detect the presence of a trace amount of palladium catalyst in the final product. Pd-catalyzed Sonogashira coupling reaction was used as a model reaction (ESI†), where the crude reaction product containing leftover Pd was added in CNPs and fluorescence quenching was observed, which is in accordance with the proposed sensing methodology (Fig. 8).

The advantages offered by CNPs over other reports[15,20,23,29] by employing citric acid as a carbon source are (i) synthesis using simple heating and nonrequirement of microwave irradiation or an electrochemical process, (ii) high quantum yield (24.9%) without using any surface passivation agent, (iii) efficient fluorescence quenching in the presence of a noble metal and

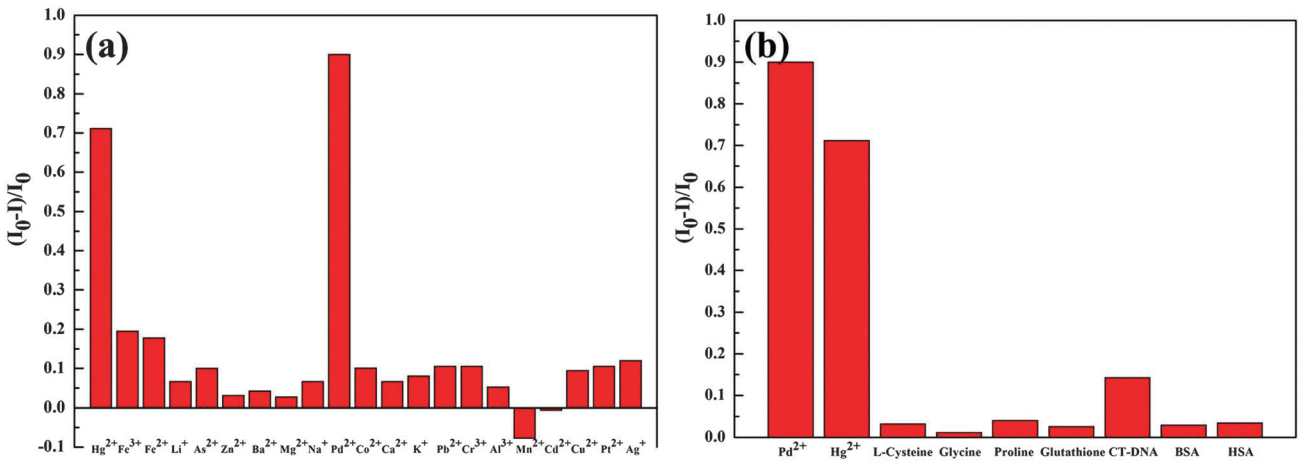

Fig. 6 Specificity of the sensor towards Pd^{2+} and Hg^{2+}.

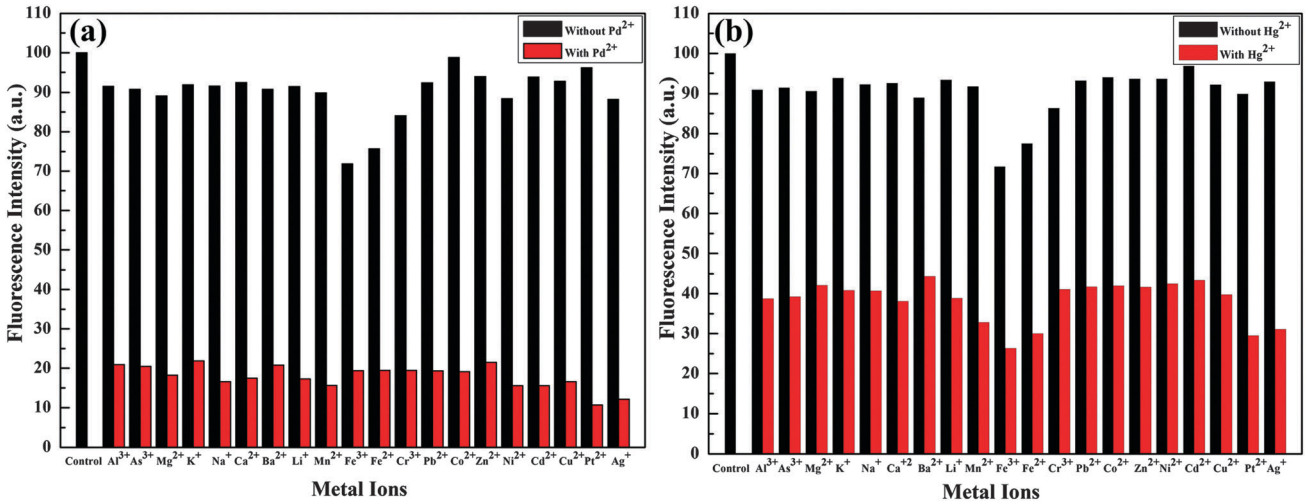

Fig. 7 Selectivity of the sensor towards Pd^{2+} and Hg^{2+} in the presence of competitive metal ions.

Table 1 Determination of Pd^{2+} and Hg^{2+} in real water samples

Metal ion	Water	Added (μM)	Measured (μM)	Recovery (%)	RSD (%)
Pd^{2+}	RO water	100	97.78	97.78	0.63
		40	39.618	99.045	0.07
	Tap water	100	98.78	98.78	0.9
		40	39.95	99.875	1.61
Hg^{2+}	RO water	18	17.46	97.04	1.01
		4	3.874	96.86	0.96
	Tap water	18	18.05	100.32	0.69
		4	4.56	114.04	1.58

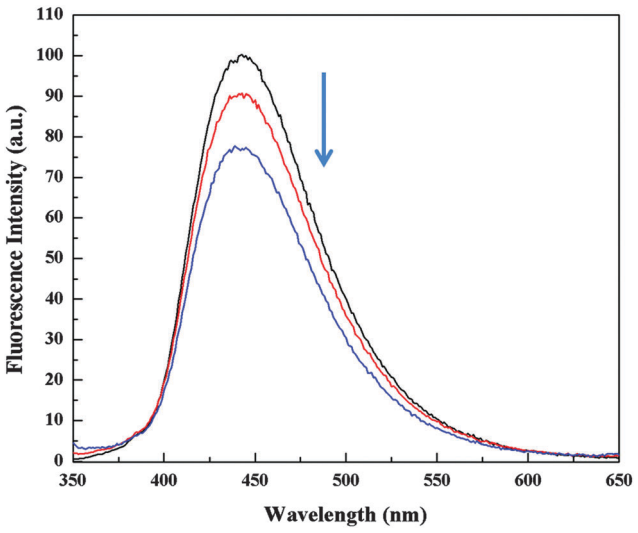

Fig. 8 Fluorescence quenching in the presence of a (Pd)-catalyzed reaction product.

heavy metal, (iv) a sensitive, selective and rapid sensing response to the detection of Pd^{2+} and Hg^{2+} in real life samples, (v) high cytocompatibility and excellent water solubility, and (vi) promising multicolour bioimaging properties along with intracellular sensing.

In comparison with the recently reported probes, our CNP based dual sensors have demonstrated better performance in terms of a broad linear range and limit of detection (Table 2).

The selective fluorescence quenching of CNPs in the presence of Hg^{2+} and Pd^{2+} may be attributed to effective chelation/coordination interactions between the metal ions and the amino, hydroxyl and carboxylic groups present in CNPs as shown in Fig. 1(d) and reported previously.[16] As obtained by TCSPC, the static quenching after coordination with Pd^{2+} can be due to the selective absorption of light by Pd^{2+}.[20] The reduced average lifetime after coordination with Hg^{2+} represents an ultra-fast electron-transfer process between CNP and Hg^{2+} which leads to dynamic quenching. Since, there is an optimum potential for electron transfer from CNPs to metal ions, the redox potential for Hg^{2+}/Hg^{+} ($\Phi = 0.91$)[16] and Pd^{2+}/Pd ($\Phi = 0.951$) is possibly optimum for electron transfer from CNPs to these ions rather than the redox potential for other metal ions M^{n+}/M.[41] Therefore, no visible quenching was observed with other metal ions and CNPs show selectivity for Hg^{2+} and Pd^{2+} over other metal ions.

Live cell imaging and cytotoxicity

Having studied the interesting photophysical properties and fluorescence response of CNPs, we anticipated the use of these CNPs as efficient biomarkers for live cell imaging. For the practical importance of such materials for bioimaging, it was significant to probe the cytotoxic effects of CNPs on live cells, thus the toxicity of CNPs was studied on two different cell lines A375 and DU145. The CNPs were found to be non-cytotoxic on the studied cell lines at concentrations as high as 100 μg mL^{-1}. The results of the MTT cytotoxicity assay are summarized in Fig. 9. The nontoxic nature of these CNPs makes them ideal materials for cell labelling.

In order to determine the capability of CNPs for bioimaging A375 and DU-145 cell lines were incubated with CNPs and the corresponding confocal fluorescence microscopic images are exhibited in Fig. 10. As illustrated, the cells treated with CNPs have shown considerable cellular uptake along with multicolor

Table 2 Performance comparison of different sensors for the detection of Pd^{2+} and Hg^{2+}

Reagent	Detection	LOD	Method	Ref.
Dabsyl-L-aspartic acid–BSA complex	Hg	0.5 μM	Fluorescence turn on	30
Acetate mediate *N*-acylation of thiourea derivative	Hg	0.6 μM	Fluorescence turn on	31
Dichlorofluorescein derivative	Hg	15 μM	Fluorescence	32
G-quadruplex based DNAzyme	Hg	100 nM	Colorimetric	33
Gold nanoparticle	Hg	2.9 nM	Colorimetric	34
Silica sphere@Au nanoparticle	Hg	0.1 nM	SERS	35
Ferrocene–graphene nanosheets	Hg	18 pM	Electrochemiluminescence	36
Carbon dots	Hg	20 nM	Fluorescence	20
Rhodamine based (Rd-Eb)	Pd	1.91×10^{-7} M	Fluorescence turn on	37
Nano-conjugate adsorbent (NCA)	Pd	0.14 μg L^{-1}	Colorimetric	38
Luminescent lanthanide complexes	Pd	80 nM	Fluorescence turn on	39
Benzoxazole ring	Pd		Fluorescence-NIR	40
Carbon nanoparticles (CNP)	Hg	100 nM	Fluorescence turn off	This work
Carbon nanoparticles (CNP)	Pd	58 nM	Fluorescence turn off	This work

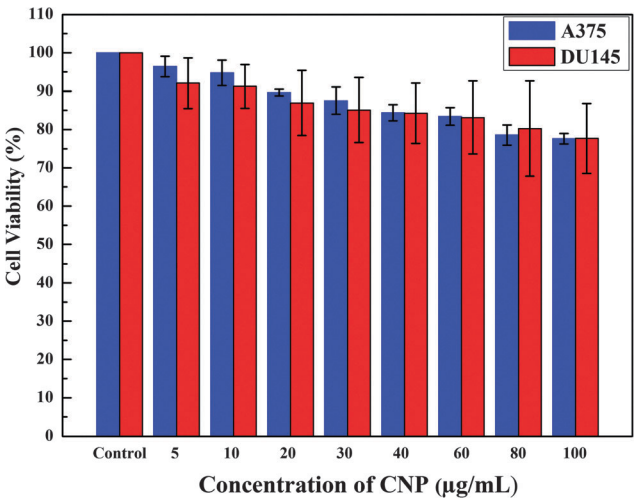

Fig. 9 Cell viability profile of carbon nanoparticles.

cell labelling. When intracellular CNPs were excited at 405 nm, 488 nm and 559 nm, fluorescence signals of blue, green and red color were observed, respectively, and the fluorescence in the cells retained high intensity (Fig. 10).

The intact morphology and healthy spread of adherent cells after the labelling process further validate the non-toxic nature of CNPs. The cellular uptake of CNPs can be attributed to their small size and hydrophilic nature, leading to the uptake by the cells, most likely through endocytosis.[42] As observed from the two channel confocal images (Fig. S3, ESI†), bright blue and green fluorescence reveals that a large amount of CNPs was internalized by the cells. The well distribution of CNPs was observed through luminescence image overlap with the phase contrast image. The emission was located throughout the cells hence it can be concluded that CNPs do not specifically stain any organelles and behave similarly for both the tested cell lines A375 and DU145. Interesting multicolour emission during bioimaging prompted us to study the wavelength tuned emission of CNPs. The fluorescence spectra of CNPs at different excitation wavelengths are shown in Fig. S4 (ESI†), which exhibit the bathochromic shift in emission wavelength with an increase in excitation.

Intracellular sensing of Pd^{2+} and Hg^{2+}

In order to assess the capability of CNP sensors to probe intracellular Pd^{2+} and Hg^{2+}, DU145 and A375 cell lines were

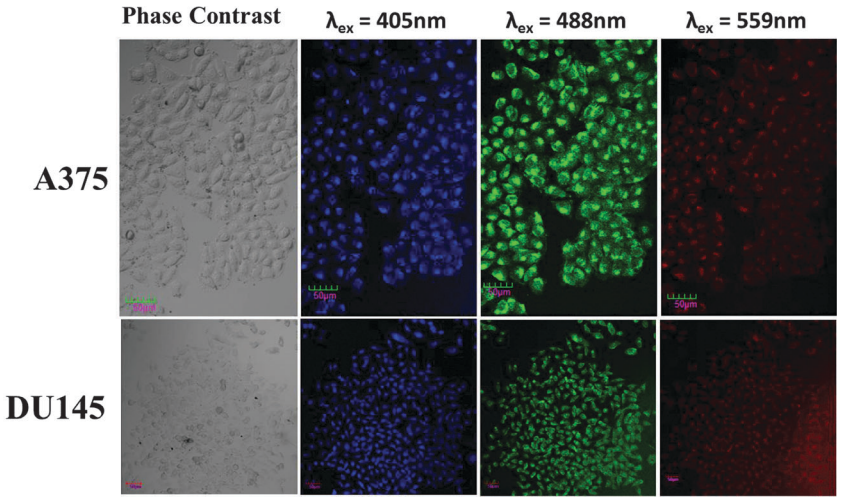

Fig. 10 Cell labelling of A375 and DU145 cancer cell lines using CNPs.

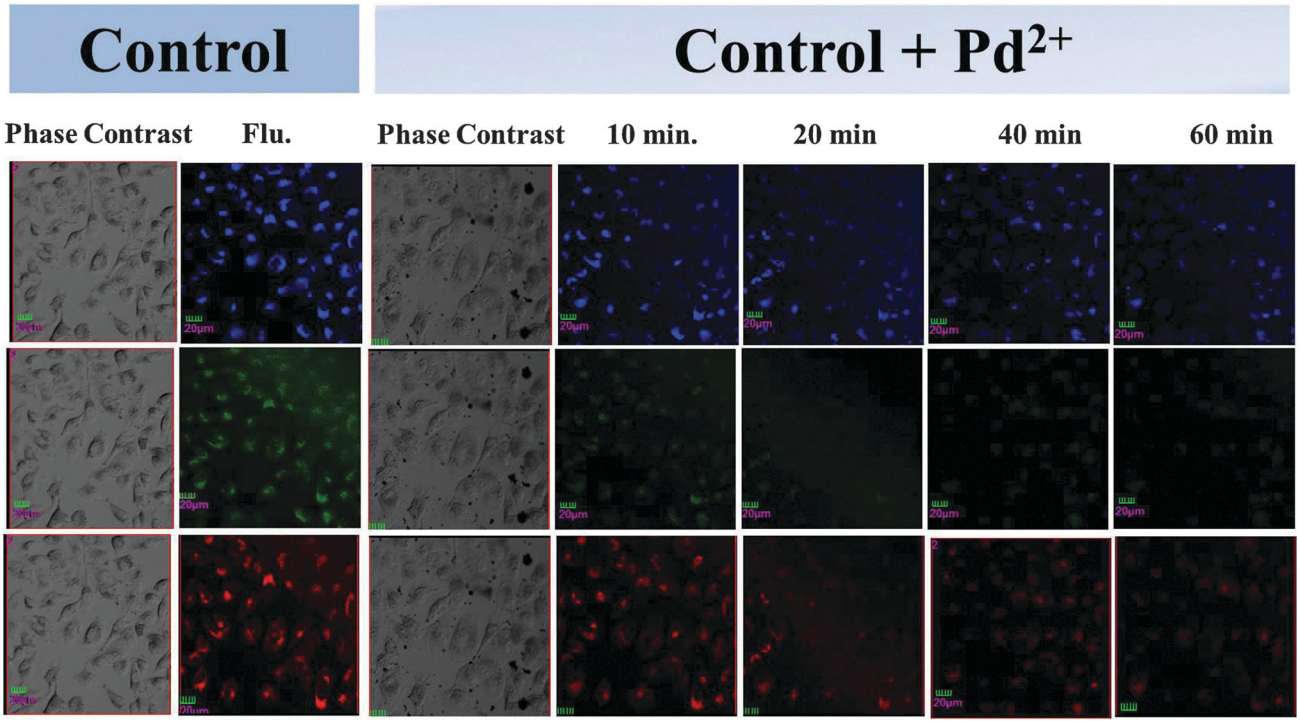

Fig. 11 The confocal microscopy images of DU145 cells treated with CNPs (control), followed by further incubation with Pd^{2+} at different time intervals.

incubated with CNPs overnight. The DU145 and A375 cell lines treated with CNPs and without metal ions were used as controls. Furthermore, Pd^{2+} or Hg^{2+} was added to control DU145 and A375, respectively, and confocal microscopy was performed over a span of 60 minutes. Fig. 11 and Fig. S5 (ESI†) show that a strong fluorescence signal was observed from control cells. In contrast, there is a significant decrease in intracellular fluorescence after treatment with Pd^{2+} or Hg^{2+}. The reduction in fluorescence intensity clearly indicates that the biocompatible CNP can serve as an intracellular nanoprobe for Pd^{2+} and Hg^{2+} detection.

It is worth mentioning here that though the CNPs were not stable under continuous UV illumination of 366 nm (Fig. 2c) they were found to be stable under visible light (Fig. 2d). Since, the wavelength used for confocal imaging is in the range of visible light *i.e.* 405 nm, 488 nm and 559 nm and the laser scan was recorded once after every 10 minutes for a total of 60 minutes, the possibility of photobleaching was minimum. To ensure this, DU145 cells were treated with CNPs and a video was recorded up to 50 scans and no visible photobleaching was observed (ESI†). Also the effect of Pd^{2+} on different areas of the cell suspension was recorded and is shown in Fig. S6 (ESI†).

Experimental section

Materials and instrumentation

Citric acid and ethylenediamine were purchased from Sigma Aldrich. Different metal salts were purchased from Merck and Sigma Aldrich. All chemicals were used as received without further purification. The water used was purified using a Sartorius Milli-Q system. A Varian Cary 100 Bio UV-visible spectrophotometer was used for absorption measurements. IR spectra [4000–400 cm^{-1}] were recorded using a Bio-Rad FTS 3000MX instrument on KBr pellets. Fluorescence studies were performed using a Fluoromax spectrofluorometer. Powder X-ray diffraction studies were carried out on a Rigaku SmartLab X-ray diffractometer using CuKα radiation (1.54 Å). SEM was done using a JSM-7600F FEG-Scanning Electron Microscope. Confocal microscopy was performed using an Olympus confocal laser scanning microscope.

Synthesis of carbon nanoparticles

Carbon nanoparticles were synthesized using citric acid as the carbon source. Briefly, citric acid (1 g) was dissolved in 10 mL water and 350 μL ethylenediamine was added to the solution and stirred vigorously for 30 minutes at room temperature to make a homogeneous mixture. The mixture was then transferred to a 23 mL Teflon autoclave which was air tightened and kept in a furnace at 250 °C for 5 hours. After cooling a yellowish brown solution was obtained, which was further diluted in water to obtain a fluorescent solution containing carbon nanoparticles.

Metal ion sensing

The palladium and mercury metal ions were detected at room temperature in water. Appropriate dilution of CNPs was made in water and different concentrations of various metal ions in water were added stepwise. Briefly, 10 μL of the as-prepared CNP was added to 42 mL of water and it served as a stock solution. This stock solution was further diluted by adding 1 mL of stock solution in 25 mL ultrapure water. Various aliquots of 2 mL of this control solution were made to which

varying concentrations of different metal ions were added. The final concentration of CNPs in all sensing experiments was 1 μg mL^{-1}. The fluorescence emission spectra were recorded within 2 minutes of addition.

Cellular toxicity and bioimaging

To determine the toxicity of the CNPs on living systems, two different cancer cell lines, skin melanoma cancer (A375) and prostate cancer (DU145) obtained from National Centre for Cell Science, Pune, were used as models.

Minimum essential medium (MEM, Himedia) was used to culture A375 cells while the DU145 cells were grown in Dulbecco's Modified Eagle's medium (DMEM). The growth medium was supplemented with 10% foetal bovine serum (FBS, Life Technologies) and antibiotics, penicillin (100 U ml^{-1}) and streptomycin (100 μg ml^{-1}). Cytotoxicity studies were carried out using the standard 3-(4,5-dimethylthiazole-2-yl)-2,5-diphenyl tetrazolium bromide (MTT) assay.[43] To perform the assay, cells were seeded into 96 well plates in triplicates at a seeding density of 5000 cells per well in 100 μL of the respective culture medium for 48 hours. Furthermore, CNPs dissolved in water were added to the wells in concentrations ranging from 0 μg mL^{-1} to 100 μg mL^{-1}. Control cells with 0 μg mL^{-1} CNPs were used in the study. The cells were further incubated for 12 hours. Afterwards, the culture medium containing CNPs was replaced with a 100 μL phenol red free fresh medium and 10 μL MTT (5 mg ml^{-1} in 1× PBS, pH 7.4) was added to each well and the cells were incubated at 37 °C for 4 hours. Subsequently, MTT incubated medium was removed from the wells and 50 μL DMSO was added to dissolve insoluble purple formazan crystals and incubated for 10 minutes in a CO_2 incubator. The absorbance at 570 nm was read using a Synergy H1 Biotek microplate reader. The cell viability was quantitated based on % cell viability using the formula: % cell viability = $Abs_{(exp)}/Abs_{(control)} \times 100$, and plotted on a bar graph using Origin 8.0.

For bioimaging, cells were seeded in confocal dishes at a density of 30 000 cells per dish and incubated for 24 h in a CO_2 incubator. Furthermore, the cells were treated with CNPs and kept for 24 h in the CO_2 incubator. The cells were then washed with 1× PBS thrice and live cell imaging was performed immediately using a confocal laser scanning microscope.

Conclusions

In summary, a one-step synthesis strategy for cytocompatible fluorescent water soluble carbon nanoparticles (CNPs) was reported. The CNPs were found to be stable in a range of temperatures, pH and time. The CNPs have shown remarkable capability of sensitive and selective detection of Pd^{2+} and Hg^{2+} among twenty different metal ions studied in an aqueous medium. The sensor was also successfully employed on real life samples. In particular, the detection of expensive Pd catalyst in a trace amount from reaction products will be highly beneficial for industries. Furthermore, CNPs were tested for potential intracellular applications where they were found to be nontoxic and effective multicolor bioimaging probes, along with the capability of sensing Pd^{2+} and Hg^{2+} in live cells. To the best of our knowledge, this is the first kind of dual sensor to be developed which probes both noble metals and heavy metals with added advantages of cytocompatibility and multicolour bioimaging.

Acknowledgements

We sincerely acknowledge Sophisticated Instrumentation Centre (SIC), IIT Indore for providing the characterization facility. We acknowledge SAIF, IIT Bombay for SEM facility. SMM would like to acknowledge CSIR, New Delhi, India for funding. VS and AKS would like to thank UGC, Govt. of India for providing research fellowship.

References

1 Y. Wang and A. Hu, *J. Mater. Chem. C*, 2014, **2**, 6921–6939.
2 A. Jaiswal, S. S. Ghosh and A. Chattopadhyay, *Chem. Commun.*, 2011, **48**, 407–409.
3 M. Algarra, M. Pérez-Martín, M. Cifuentes-Rueda, J. Jiménez-Jiménez, J. C. G. Esteves da Silva, T. J. Bandosz, E. Rodríguez-Castellón, J. T. López Navarrete and J. Casado, *Nanoscale*, 2014, **6**, 9071.
4 X. Gong, W. Lu, Y. Liu, Z. Li, S. Shuang, C. Dong and M. M. F. Choi, *J. Mater. Chem. B*, 2015, **3**, 6813–6819.
5 J. Feng, W.-J. Wang, X. Hai, Y.-L. Yu and J.-H. Wang, *J. Mater. Chem. B*, 2016, **4**, 387–393.
6 A. R. Chowdhuri, S. Tripathy, C. Haldar, S. Roy and S. K. Sahu, *J. Mater. Chem. B*, 2015, **3**, 9122–9131.
7 M. Xue, M. Zou, J. Zhao, Z. Zhan and S. Zhao, *J. Mater. Chem. B*, 2015, **3**, 6783–6789.
8 D. Keum, S. Kim and Y. Kim, *Chem. Commun.*, 2014, **50**, 1268–1270.
9 F. Song, A. L. Garner and K. Koide, *J. Am. Chem. Soc.*, 2007, **129**, 12354–12355.
10 W. X. Ren, T. Pradhan, Z. Yang, Q.-Y. Cao and J. S. Kim, *Sens. Actuators, B*, 2012, **171–172**, 1277–1282.
11 H. Li, J. Fan and X. Peng, *Chem. Soc. Rev.*, 2013, **42**, 7943–7962.
12 G. V. Ramesh and T. P. Radhakrishnan, *ACS Appl. Mater. Interfaces*, 2011, **3**, 988–994.
13 A. K. Saini, M. Srivastava, V. Sharma, V. Mishra and S. M. Mobin, *Dalton Trans.*, 2016, **45**, 3927–3935.
14 J. Hou, J. Li, J. Sun, S. Ai and M. Wang, *RSC Adv.*, 2014, **4**, 37342–37348.
15 Y. Hou, Q. Lu, J. Deng, H. Li and Y. Zhang, *Anal. Chim. Acta*, 2015, **866**, 69–74.
16 J. Yu, N. Song, Y.-K. Zhang, S.-X. Zhong, A.-J. Wang and J. Chen, *Sens. Actuators, B*, 2015, **214**, 29–35.
17 D. Pan, J. Zhang, Z. Li, C. Wu, X. Yan and M. Wu, *Chem. Commun.*, 2010, **46**, 3681–3683.
18 Y. Zhao, L. Shi, J. Fang and X. Feng, *Nanoscale*, 2015, **7**, 20033–20041.

19 S. K. Bhunia, A. Saha, A. R. Maity, S. C. Ray and N. R. Jana, *Sci. Rep.*, 2013, **3**, 1473.
20 Y. Zhai, Z. Zhu, C. Zhu, J. Ren, E. Wang and S. Dong, *J. Mater. Chem. B*, 2014, **2**, 6995–6999.
21 Y. Li, X. Zhong, A. E. Rider, S. A. Furman and K. (Ken) Ostrikov, *Green Chem.*, 2014, **16**, 2566–2570.
22 S. Qu, X. Wang, Q. Lu, X. Liu and L. Wang, *Angew. Chem., Int. Ed.*, 2012, **51**, 12215–12218.
23 H. Zhu, X. Wang, Y. Li, Z. Wang, F. Yang and X. Yang, *Chem. Commun.*, 2009, 5118–5120.
24 R. Liu, D. Wu, S. Liu, K. Koynov, W. Knoll and Q. Li, *Angew. Chem., Int. Ed.*, 2009, **48**, 4598–4601.
25 H. Peng and J. Travas-Sejdic, *Chem. Mater.*, 2009, **21**, 5563–5565.
26 Y. Yang, J. Cui, M. Zheng, C. Hu, S. Tan, Y. Xiao, Q. Yang and Y. Liu, *Chem. Commun.*, 2011, **48**, 380–382.
27 H. Li, X. He, Z. Kang, H. Huang, Y. Liu, J. Liu, S. Lian, C. H. A. Tsang, X. Yang and S.-T. Lee, *Angew. Chem., Int. Ed.*, 2010, **49**, 4430–4434.
28 A. Shrivastava and V. Gupta, *Chron. Young Sci.*, 2011, **2**, 21.
29 X. Zhai, P. Zhang, C. Liu, T. Bai, W. Li, L. Dai and W. Liu, *Chem. Commun.*, 2012, **48**, 7955–7957.
30 L.-J. Ma, Y. Li, L. Li, J. Sun, C. Tian and Y. Wu, *Chem. Commun.*, 2008, 6345.
31 X. Lu, Z. Guo, M. Feng and W. Zhu, *ACS Appl. Mater. Interfaces*, 2012, **4**, 3657–3662.
32 M. G. Choi, D. H. Ryu, H. L. Jeon, S. Cha, J. Cho, H. H. Joo, K. S. Hong, C. Lee, S. Ahn and S.-K. Chang, *Org. Lett.*, 2008, **10**, 3717–3720.
33 T. Li, B. Li, E. Wang and S. Dong, *Chem. Commun.*, 2009, 3551–3553.
34 L. Chen, J. Li and L. Chen, *ACS Appl. Mater. Interfaces*, 2014, **6**, 15897–15904.
35 M. Liu, Z. Wang, S. Zong, H. Chen, D. Zhu, L. Wu, G. Hu and Y. Cui, *ACS Appl. Mater. Interfaces*, 2014, **6**, 7371–7379.
36 B. Zhuo, Y. Li, A. Zhang, F. Lu, Y. Chen and W. Gao, *J. Mater. Chem. B*, 2014, **2**, 3263–3270.
37 F. Liu, J. Du, M. Xu and G. Sun, *Chem. – Asian J.*, 2016, **11**, 43–48.
38 M. R. Awual, M. M. Hasan and H. Znad, *Chem. Eng. J.*, 2015, **259**, 611–619.
39 E. Pershagen, J. Nordholm and K. E. Borbas, *J. Am. Chem. Soc.*, 2012, **134**, 9832–9835.
40 W. Chen, B. D. Wright and Y. Pang, *Chem. Commun.*, 2012, **48**, 3824–3826.
41 A. Zhu, Q. Qu, X. Shao, B. Kong and Y. Tian, *Angew. Chem., Int. Ed.*, 2012, **51**, 7185–7189.
42 P. G. Luo, S. Sahu, S.-T. Yang, S. K. Sonkar, J. Wang, H. Wang, G. E. LeCroy, L. Cao and Y.-P. Sun, *J. Mater. Chem. B*, 2013, **1**, 2116–2127.
43 J. Carmichael, W. G. DeGraff, A. F. Gazdar, J. D. Minna and J. B. Mitchell, *Cancer Res.*, 1987, **47**, 936–942.

